Biosensors and Bioelectronics 131 (2019) 60–66

Contents lists available at ScienceDirect

Biosensors and Bioelectronics

journal homepage: www.elsevier.com/locate/bios

Turbidimetric inhibition immunoassay revisited to enhance its sensitivity via an optofluidic laser

Xi Yang[a], Wenxiong Shu[a], Yanqiong Wang[a], Yuan Gong[a,*], Chaoyang Gong[a], Qiushu Chen[b], Xiaotian Tan[b], Gang-Ding Peng[c], Xudong Fan[b], Yun-Jiang Rao[a,*]

[a] Key Laboratory of Optical Fiber Sensing and Communications (Ministry of Education of China), University of Electronic Science and Technology of China, Chengdu, Sichuan 611731, China
[b] Department of Biomedical Engineering, University of Michigan, Ann Arbor, MI 48109, USA
[c] School of Electrical Engineering and Telecommunications, University of New South Wales, Sydney, NSW 2052, Australia

ARTICLE INFO

Keywords:
Optofluidic laser
Turbidimetric inhibition immunoassay
Laser dye
Antigen-antibody complexes
Biomarker detection

ABSTRACT

Turbidimetric inhibition immunoassay (TIIA) is a classic immunodiagnostic method that has been extensively used for biomarker detection. However, the low sensitivity of this technique hinders its applications in the early diagnosis of diseases. Here, a new concept, optofluidic laser TIIA (OFL-TIIA), is proposed and demonstrated for sensitive protein detection. In contrast to the immunoreaction in traditional TIIA, in which the single-pass laser loss is detected, the immunoreaction in the OFL-TIIA method takes place in a laser cavity, which considerably increases the loss induced by antigen-antibody complexes (AACs) via the amplification effect of the laser. A commercial IgG TIIA kit was selected as a demonstrative model to characterize the performance of OFL-TIIA. A wide dynamic range of five orders of magnitude with an exceptional limit of detection (LOD) (1.8×10^{-10} g/L) was achieved. OFL-TIIA is a fast, sensitive, and low-cost immunoassay with a simple homogeneous and wash-free process and low-volume sample consumption, thus providing a new detection platform for disease diagnostics.

1. Introduction

The turbidimetric inhibition immunoassay (TIIA) is a classic analytical tool (Libby, 1938) used for various biological applications, such as monitoring of bacterial growth rate (Hall et al., 2013) and specific quantification of protein concentration (Ferreria and Price, 1974). In TIIA, an antibody is mixed with its target antigen to form antigen-antibody complexes (AACs) in bulk solution. Once a strong electrolyte is added, AACs aggregate into large complexes that cannot dissolve in water and form a suspension (Harmoinen et al., 1981; Otsuji et al., 1982; Holownia et al., 2001; Wu et al., 2000). The antigen concentration can be measured by detecting the transmittance of a laser through the aggregated AACs. Compared to a surface-conjugated immunoassay, e.g., ELISA, TIIA is wash-free, making it unique and highly competitive (Culver et al., 2017). Owing to the high specificity of antigen-antibody binding, the homogeneous reaction, and the rapidness of the assay (< 20 min) (Deleo et al., 1991), TIIA has been employed to measure proteins in clinics for decades (Kjelgaard-Hansen et al., 2004; Chan, 1995; Hillstrom et al., 2014), and its impact is reflected by the various commercial TIIA analyzers and kits available from companies worldwide (Roche, Randox, etc.).

However, the traditional TIIA (T-TIIA) has its drawbacks. First, its low sensitivity limits its use in applications that require highly sensitive assays, such as the early diagnosis of diseases. Second, the dynamic range for TIIA is generally too narrow to detect biomarkers that may change over several orders of magnitude. Third, TIIAs are usually performed in a quartz cuvette and require large sample/reagent volumes (~2 mL), resulting in a relatively high cost. Great efforts have been made to enhance TIIA sensitivity, including TIIAs enhanced by latex particles (Nishimura and Sawai, 2006), erythrocytes (Srihirun et al., 2012), and gold sols (Thanh and Rosenzweig, 2002). However, all of these experimental demonstrations were focused on the conjugation of the antibody/antigen to nanomaterials or cells, which makes the biochemical process relatively complicated. From the perspective of the detection scheme, the sensitivity of the assay was not enhanced, as the T-TIIA method was used.

Optofluidic lasers (Shopova et al., 2007; Gersborg-Hansen and Kristensen, 2006; Li et al., 2006; Arango et al., 2007; Gong et al., 2017a, 2017b, 2018) are emerging as a highly sensitive tool for detecting biological processes at the molecular, cellular, and tissue levels (Gather and Yun, 2011; Humar and Yun, 2015; Fan and Yun, 2014; Wu et al., 2014; Q. Chen et al., 2017; Y.C. Chen et al., 2017b, 2018). In this study,

* Correspondence to: No. 2006, Xiyuan Ave., High-Tech Zone (West), Chengdu, Sichuan 611731, China.
E-mail addresses: ygong@uestc.edu.cn (Y. Gong), yjrao@uestc.edu.cn (Y.-J. Rao).

https://doi.org/10.1016/j.bios.2019.02.013
Received 30 November 2018; Received in revised form 25 January 2019; Accepted 4 February 2019
Available online 19 February 2019
0956-5663/

we developed a highly sensitive optofluidic laser TIIA (OFL-TIIA) that can detect analytes at low concentrations within a large dynamic range. Compared to T-TIIA, OFL-TIIA incorporates biomaterials into the gain solution, which enhances the light-matter interaction through an optical microresonator. Therefore, the laser intensity decreases sharply with increasing sample concentration, and a high sensitivity for biomarker detection can be achieved due to the laser amplification effect. In general, OFL-TIIA maintains the advantages of both TIIA and an optofluidic laser, including being wash-free and having high sensitivity. Rhodamine B (RhB), which is biocompatible, water-soluble and lasing wavelength tunable, was employed as the gain medium for the optofluidic laser. A commercial IgG TIIA kit was used as a model to demonstrate the sensing performance of the OFL-TIIA. The experimental results indicate that OFL-TIIA is superior to T-TIIA, optofluidic-improved traditional TIIA (OIT-TIIA) and Fabry-Perot (FP) cavity-enhanced fluorescence TIIA (CEF-TIIA), as a dynamic range of five orders of magnitude with a limit of detection (LOD) of 1.8×10^{-10} g/L was achieved. In addition to its inherent advantages namely, its low cost, low-volume sample consumption, wash-free procedure, and fast and homogeneous reaction, this work provides a sensitive immunoassay platform by reinventing the TIIA.

2. Materials and methods

2.1. Apparatus

A schematic diagram of the experimental setup for OFL-TIIA is illustrated in Fig. 1a. An optofluidic FP cavity was constructed by two reflective mirrors (Thorlabs, USA) with reflectivities of 91.5% (upper) and 99.5% (bottom), which were aligned by two silica capillaries (Friedrich & Dimmock Inc., 1.1 mm × 1.1 mm inner square cross section, 0.3 mm wall thickness) sandwiched between the two mirrors. The mixture of AACs and the gain medium was withdrawn into the microfluidic capillary and pumped by the 532 nm pulsed laser (CNI Laser Inc., China) with an 8.5 ns pulsed width and a 20 Hz repetition rate. The optofluidic laser emission was collected by a lens and sent to a portable spectrometer (Ocean Optics, USA) via a multimode optical fiber. The acquisition time for the spectrometer was set at 2 s. To enhance the signal-to-noise ratio, an edge filter was added along with the collection lens to remove the residual pump at 532 nm, and a 2 OD neutral density filter was employed to attenuate the fluorescence background and to avoid saturation of the spectrometer. In addition, the pump beam in OFL-TIIA was incident from the edge of the upper mirror, and the pump energy density was above the lasing threshold (Figs. S1c-f). By contrast, the laser pump in CEF-TIIA was irradiated on the microfluidic channel by transmitting through the upper mirror, and the pump energy density was below the lasing threshold.

For comparison with T-TIIA, a He-Ne laser beam (632.8 nm) was transmitted through the cuvette once, and the transmittance was measured by a photodetector to determine the antigen concentration (Fig. S1a). By replacing the cuvette and He-Ne laser with a capillary and an optofluidic laser, respectively (Fig. S1b), OIT-TIIA was developed in order to reduce the sample volume and thus lower the cost. In this case, the sample capillary outside the FP cavity was spatially separated from the gain materials.

2.2. The principle of TIIA

AACs are derived from a reversible immunoreaction between an antibody and an antigen, whose concentration varies with the ratio of the antigen to antibody. Fig. 1b qualitatively describes the AAC concentration versus the antigen concentration in TIIA. The shape of the curve is dependent on the species of the antibody and on its avidity for the antigen. According to the number of antibody binding sites, three regions are defined, i.e., antigen excess, equivalence, and antibody excess regions (Whicher et al., 1982). Our experiment is performed in the antibody excess region. As there are sufficient antibody molecules for the immunoreaction, both the size and concentration of AACs would increase with an increase in the number of antigen molecules. Moreover, we use polyethylene glycol (PEG) to reduce the solubility of AACs by exclusion of water and further enhance the turbidity as well as the sensitivity (Fig. 1c).

Upon passing through the AAC suspension, the incident light would be attenuated because of scattering, absorption, and reflection. The

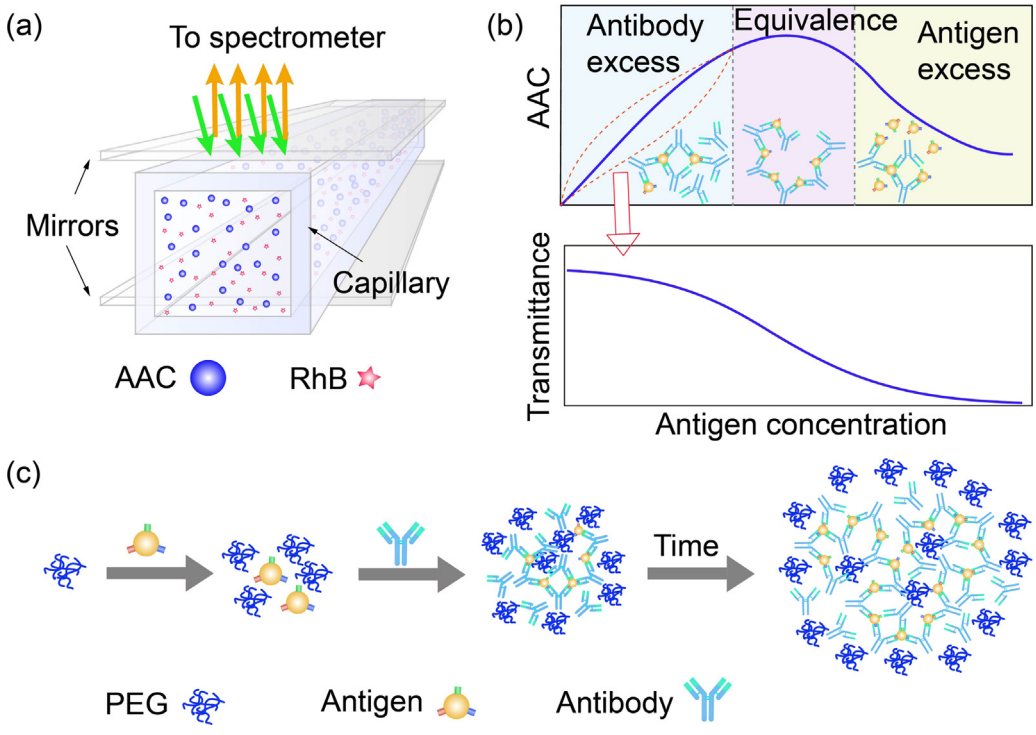

Fig. 1. (a) Schematic diagram of OFL-TIIA. (b) The principle of TIIA. (c) Experimental procedure to form AACs.

intensity attenuation changes with the AAC concentration according to the Beer-Lambert law, i.e., $I_T = I_0 e^{-\alpha_s C_{AAC} L}$, where I_T and I_0 are the intensity of transmitted light and incident light, respectively; α_s is the scattering coefficient; C_{AAC} is the AAC concentration; and L is the path length. The intensity attenuates linearly with the AAC concentration on a semi-logarithmic scale, and a similar trend is observed for the antigen concentration. Thus, in the antibody excess region, the antigen concentration can be determined by the laser intensity (Fig. 1b).

2.3. Reagents

A commercial IgG kit for the immunoturbidimetric assay was purchased from Erkn, China. It contains 100 mM tri-hydroxy methyl amino methane buffer (Tris buffer), 40 g/L PEG, goat anti-rabbit IgG, 0.95 g/L sodium azide (NaN_3), and sample IgG. RhB was purchased from Aladdin Biotech Co., Ltd., China, and was of high-performance liquid chromatography (HPLC) grade. Sodium hypochlorite (NaClO) was of analytical grade. Tris buffer and Milli-Q water ($R = 18.2\,\Omega$) were used throughout the experiment.

2.3.1. Preparation of RhB

RhB was selected as the gain medium in this experiment, as its lasing wavelength is close to 600 nm (Li et al., 2015), as required by the TIIA kits for attenuation detection. The RhB stock solution (1.5 mM) was prepared by dissolving RhB powder in Milli-Q water at room temperature. Then, the RhB stock solution was diluted in Tris buffer (100 mM) at different concentrations to optimize the emission wavelength for TIIA.

2.3.2. Preparation of AAC suspension

The TIIA protocol in this research follows the procedure described in the kits. The working solution of concentrated IgG standard was diluted daily with Milli-Q water to achieve a 10-fold series of concentrations. Next, 10 μL of IgG standard solution with a certain concentration was mixed with 1125 μL of Tris-PEG buffer and incubated at 37 °C for 5 min (solution A). A total of 375 μL of the antibody solution was added to solution A and incubated at 37 °C for 10 min to acquire the AAC suspension (solution B). Then, solutions A and B were ready for subsequent TIIA experiments. Compared to the gold standard immunoassay, ELISA, TIIA is much simpler in terms of reagent preparation and has a faster immunoreaction due to its inherent homogeneous property.

2.3.3. OFL-TIIA and CEF-TIIA

A 1.2 mM RhB solution was mixed with solution B at a volume ratio of 1:9. Then, the mixture was injected into the capillary in the FP cavity (Fig. 1a). After each test, the mixture of RhB and AAC solutions was extracted out, and the capillary was rinsed with Milli-Q water followed by a NaClO solution (10 min of incubation) and Milli-Q water (3 min of incubation). Compared to surface-attached immunoreactions, the immunoreaction in these techniques takes place in bulk solution, making it easy to remove the residual RhB and AAC in the capillaries.

2.3.4. OIT-TIIA

The optimal RhB working solution (0.12 mM) was injected into the gain capillary within the FP cavity, and solution B was withdrawn into the sample capillary (Fig. S1b). The wash protocol for the sample capillary was the same as that for the capillary in OFL-TIIA, while the gain capillary was washed with Milli-Q water for 10 min of incubation.

3. Results and discussion

3.1. Characterization of optofluidic laser

A 0.12 mM RhB/Tris buffer solution was employed as the gain medium to characterize the optofluidic laser. As shown in Fig. 2a, the lasing emission peaks gradually emerged with increasing pump energy density. The inset of Fig. 2b shows that the full-width at half-maximum (FWHM) of the optofluidic laser was approximately 3 nm, which is much narrower than that of fluorescence. The spectrally integrated intensity is plotted as a function of the pump energy density (Fig. 2b), demonstrating a laser threshold of 23.9 μJ/mm^2. The relatively low laser threshold is beneficial for the sensitivity of the immunoassay and makes the optofluidic laser applicable as a high-intensity light source for TIIA.

3.2. Experimental parameters

The experimental parameters, including the pH of the solution, the lasing wavelength, and the incubation time, are critical to achieve high performance of the sensor.

3.2.1. pH value

TIIA requires the pH value to be maintained in the range from 6 to 8 and thus the Tris buffer is used as solvent. Considering the biocompatibility of the dye solution, dye diluted with Tris buffer preserved the pH and ion concentration of solutions when it was mixed with the TIIA reagents during the immunoassay.

3.2.2. Laser wavelength

The TIIA kit requires the laser wavelength to be close to 600 nm for the turbidity-induced laser loss measurement. Notably, the laser wavelength of dye lasers can be tuned by the dye concentration (Lacey et al., 2007). Thus, the RhB stock solution was diluted with Tris buffer to various concentrations, and the corresponding laser spectra were recorded (Fig. 2c). The laser peak wavelength redshifted due to reabsorption (Dhami et al., 1995) with increasing dye concentration and was saturated at approximately 596 nm with 0.12 mM RhB (Fig. 2d). Considering RhB consumption, the pump energy density, and the optofluidic laser linewidth, 0.12 mM RhB was selected as the optimal working concentration.

3.2.3. Incubation time

The incubation time for TIIA was evaluated. In general, too short of an incubation time would cause additional error arising from manual operation and may also limit the dynamic range. In addition, too long of an assay time is not preferable for clinical use. A compromise of a 10 min incubation time was established for the following experiments. Details will be given in the next section.

3.3. OIT-TIIA and CEF-TIIA

To compare different schemes of TIIA, we experimentally evaluated T-TIIA, OIT-TIIA, CEF-TIIA and finally OFL-TIIA. The experimental results indicate that T-TIIA and OIT-TIIA have similar sensitivity to the commercial biochemical analyzer. Compared to those of T-TIIA and OIT-TIIA, the CEF-TIIA sensing performance is improved, and the OFL-TIIA sensing performance is significantly improved.

To verify the principle of TIIA, the temporal variation in laser transmittance was recorded via the T-TIIA setup at various IgG concentrations (Fig. S2a). Due to the turbidimetric immunoreaction, the laser loss increases with the reaction time and eventually reaches a balance. Therefore, a reaction time of 10 min was selected as a compromise between the assay speed and sensitivity. The laser transmittance versus the IgG concentration was measured at 10 min as the standard curve (Fig. S2b), indicating that T-TIIA has low sensitivity and a limited dynamic range.

The OIT-TIIA setup, which was constructed by an optofluidic laser, had two improvements over the T-TIIA setup. First, the laser wavelength was tuned to 596 nm by dye concentration optimization (0.12 mM) to match the wavelength required for TIIA. Second, the sample volume was much lower in OIT-TIIA (5 μL) than that in T-TIIA

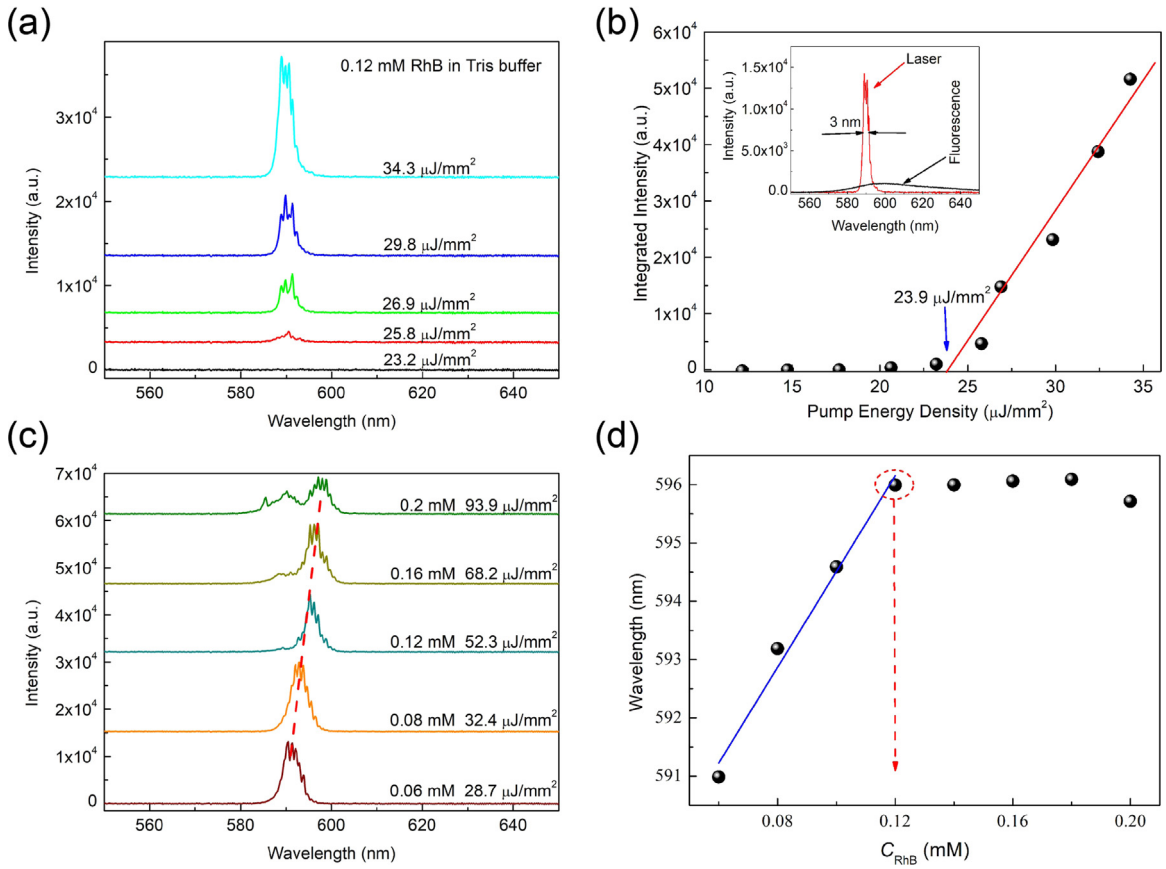

Fig. 2. Lasing characteristics of the optofluidic laser. (a) Laser spectra and (b) the spectrally integrated intensity as a function of the pump energy density, showing a threshold of 23.9 μJ/mm^2. (c) Laser spectra and (d) lasing wavelength of the optofluidic laser with different RhB concentrations. An optimized wavelength of 596 nm was obtained with 0.12 mM RhB.

(2 mL). For quantitative detection of IgG, the spectra of the laser after passing through the sample capillary with the AAC solution were recorded at different IgG concentrations (Fig. 3a). The relationship between the spectrally integrated intensity and the IgG concentration is shown in Fig. 3b. The laser intensity is kept almost constant as the IgG concentration increases until a relatively high concentration is reached. The sensitivity and dynamic range shown in Fig. 3b are similar to those of T-TIIA (Fig. S2b) and the AU-480 biochemical analyzer (Beckman Coulter, USA) (Fig. S3), which is ascribed to the compromise among the wavelength, path length, and incubation time in the three schemes.

Further improvement in the sensing performance is desirable and requires a novel method for enhancing the sensitivity. Therefore, we developed FP cavity-enhanced TIIA methods, including CEF-TIIA and OFL-TIIA. In both methods, an FP cavity consisting two reflective mirrors was employed for multiplying the path length, and the photon lifetime in the cavity was extended by bouncing the photons back and forth. The unique difference between the two techniques is whether the population inverse is achieved. OFL-TIIA will be discussed in detail in the next section.

CEF-TIIA was performed to evaluate the enhancement factor of the optical cavity. With the FP cavity, the peak wavelength of fluorescence redshifted (inset of Fig. 3c) due to reabsorption (Dhami et al., 1995). The FP-enhanced fluorescence spectra and corresponding standard curve are shown in Fig. 3c and d. The fluorescence intensity gradually decreases as the IgG concentration increases, which is similar to the trend observed in T-TIIA. Compared to T-TIIA and OIT-TIIA, CEF-TIIA exhibits an improved dynamic range of three orders of magnitude (1.8×10^{-4} g/L to 1.8×10^{-1} g/L) along with better sensitivity. The cavity enhancement factor (CEF) can be calculated as (Zhu et al., 2017)

$$CEF = \frac{1}{1 - \sqrt{R_1 R_2}} \quad (1)$$

Here, R_1 and R_2 are the reflectivities of the upper and bottom mirrors, respectively. The CEF was calculated to be approximately 21, equivalent to a path length of 23.1 mm, which clarifies the reason why CEF-TIIA provides improved sensing performance.

3.4. OFL-TIIA

OFL-TIIA was developed based on cavity-enhanced TIIA and by further pumping above the threshold. Compared to those in T-TIIA (mL level), the ultralow volumes of sample (2 μL) and reagents (6 μL) for each test in OFL-TIIA are almost three orders of magnitude less. Under the experimental conditions explored in Section 3.2, the immunoassay performance of OFL-TIIA was evaluated in buffer. The laser spectra at different IgG concentrations for OFL-TIIA were recorded (Fig. 4a). The pump energy density was fixed at 35.4 μJ/mm^2, well above the threshold of 23.9 μJ/mm^2. Fig. 4b shows the standard curve for OFL-TIIA, indicating the optofluidic laser intensity decreases linearly with increasing IgG concentration on a semi-logarithmic scale ($R^2 = 0.98$). The good interassay repeatability of the OFL-TIIA was confirmed by the small error bars from triplicate tests. A wide dynamic range of five orders of magnitude with a minimum distinguishable concentration (LOD) of 1.8×10^{-10} g/L was achieved. The sensing performance was much better than that of most IgG detection technologies (Table 1).

The significantly improved immunoassay performance of OFL-TIIA is mainly attributed to two factors. First, the use of an optical cavity extends the optical path length by 21-fold via multiple reflections. Second, the amplification effect of the laser, which mixes the gain with reagents in the resonator, further improves the performance, which can

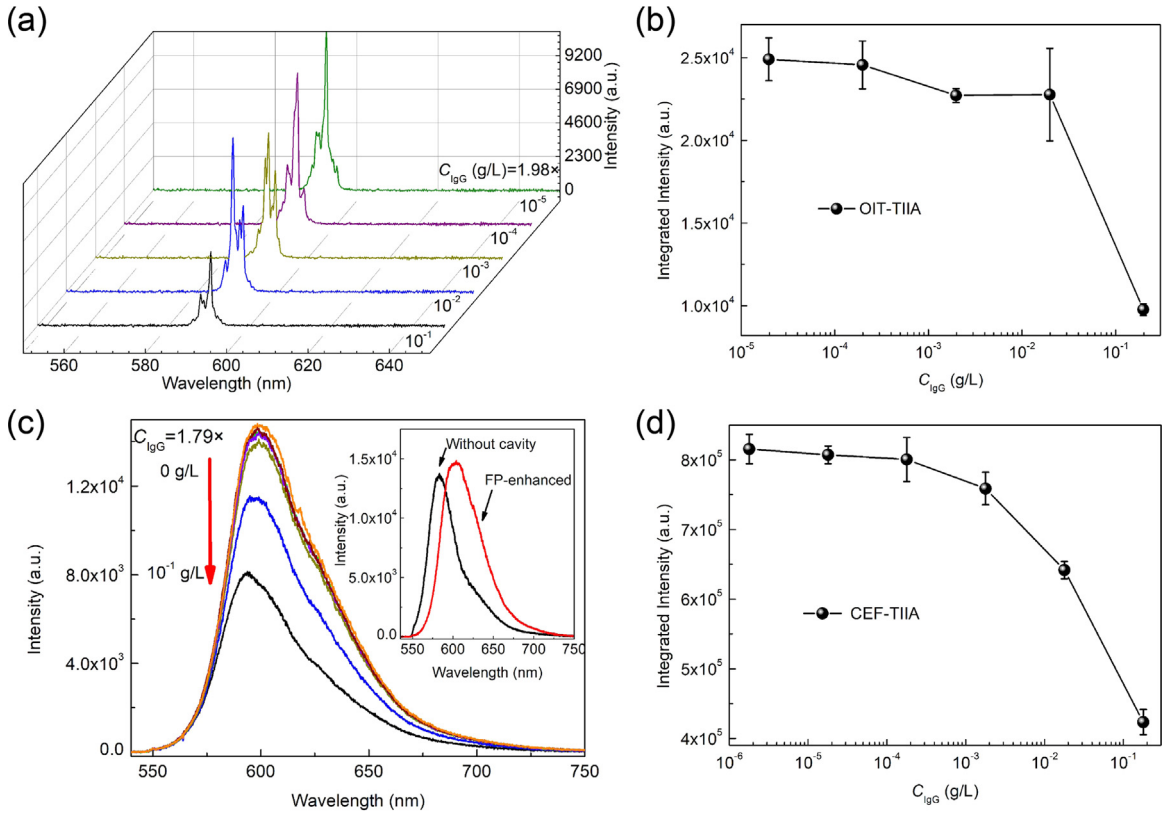

Fig. 3. (a) The laser and (c) fluorescence transmission spectra at various IgG concentrations and the corresponding standard curves for (b) OIT-TIIA and (d) CEF-TIIA. The standard curves were obtained by calculating the spectrally integrated intensity versus the IgG concentration. Inset of (c) shows the fluorescence spectra with and without an FP cavity.

be proven by a comparison with CEF-TIIA. Herein, a theoretical model was established to explain this improvement in principle (Fig. 5a). To simplify the theoretical model, we assume that only the scattering light at 0° can oscillate inside the optical cavity. Therefore, according to the Rayleigh scattering theory, the transmitted light intensity is given by (Whicher et al., 1982)

$$I_T = I_0 \frac{16\pi^4 \varepsilon^2}{\lambda^4 r^2} \tag{2}$$

Here, I_0 is the incident light intensity, ε is the molecular polarizability, and λ is the wavelength of the laser. r is the average distance between the AAC molecules. We further assume that $N_{AAC} = aN_{IgG}$, in which N_{AAC} and N_{IgG} are the numbers of AAC and IgG molecules, respectively, and a is a coefficient describing the relationship between the concentrations of AAC and IgG molecules. Hence, the average distance r is estimated to be $r = \sqrt[3]{\frac{M_{IgG}}{aN_A C_{IgG}}}$. Here, M_{IgG}, N_A and C_{IgG} are the IgG molecular weight, Avogadro constant and IgG concentration, respectively. Then, in combination with the Beer-Lambert law in Section 2.2, the scattering coefficient α_s can be calculated.

Furthermore, the laser intensity increases/decreases with the gain/loss and can be expressed as (Siegman, 1986; Wu et al., 2014)

$$I_{laser} = \frac{\delta_e I_{sat}}{2}\left(\frac{2gL}{2(\alpha_0 + C_{AAC}\alpha_s)L + \delta_e} - 1\right) \tag{3}$$

Here, $\delta_e = (1 - R_1) + (1 - R_2)$ is the external coupling factor (R_1 and R_2 are the reflectivities of the two mirrors in the FP cavity). $I_{sat} = \frac{h\omega}{\sigma\tau_{eff}}$ is the saturation intensity (h is the Planck constant, ωZ is the emission

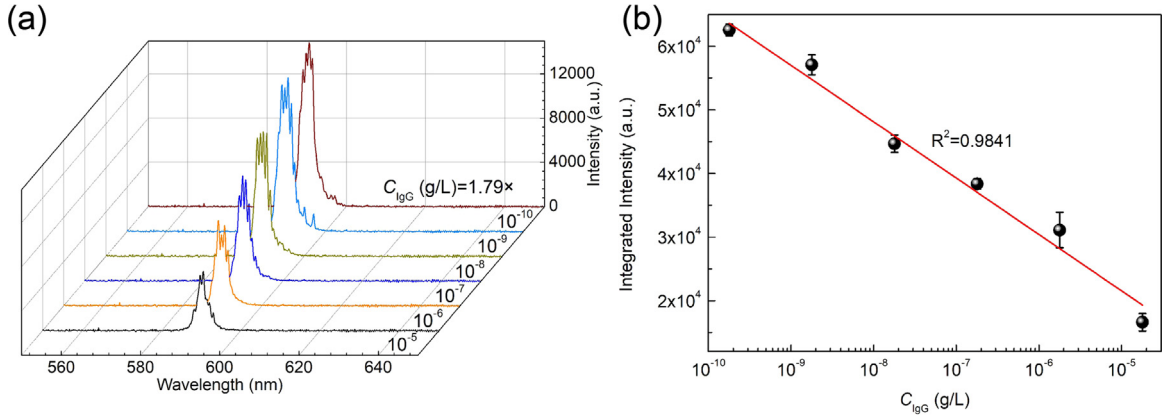

Fig. 4. (a) The laser spectra at various IgG concentrations for OFL-TIIA. (b) The spectrally integrated intensity versus the IgG concentration, i.e., the standard curve for OFL-TIIA. The error bars are based on triplicate tests.

Table 1
Comparison of the performance of different IgG detection methods.

Technology platform	Sensing principle	Detection limit (g/L)	Dynamic range (g/L)	Dynamic range, $10Log_{10}$ (C_{max}/C_{min})[a]	References
PCR	Absorption	4.56×10^{-7}	4.56×10^{-7}-4.56×10^{-4}	30	Morin et al. (2011)
SPR	Polarization Absorption	6.25×10^{-5}	6.25×10^{-5}-2.5×10^{-2}	26	Jiang et al. (2017)
	RI	6×10^{-4}	6×10^{-4}-4×10^{-2}	18.2	Zhang et al. (2016)
Electrochemical	Differential Pulse Voltammetry	9×10^{-10}	5×10^{-9}-1×10^{-4}	43	Zhang et al. (2017)
	Impedance Spectroscopy	1.4×10^{-6}	1.4×10^{-6}-2.78×10^{-5}	13	Montes et al. (2016)
	Amperometric	1.42×10^{-4}	5×10^{-4}-1×10^{-3}	3	Rosales-Rivera et al. (2012)
	Amperometric	5×10^{-6}	5×10^{-6}-2×10^{-4}	16	Wilson (2005)
	Differential Pulse Voltammetry	8×10^{-8}	1×10^{-7}-1×10^{-4}	30	Li et al. (2014)
	Differential Pulse Voltammetry	3×10^{-8}	1×10^{-7}-4×10^{-4}	36	Dong et al. (2017)
	Impedance Spectroscopy	3×10^{-7}	3×10^{-7}-3×10^{-4}	30	Subramanian et al. (2014)
	Impedance Spectroscopy	1×10^{-5}	1×10^{-5}-5×10^{-3}	27	Mashazi et al. (2013)
	Impedance Spectroscopy	3×10^{-7}	5×10^{-7}-4.5×10^{-5}	19.5	Zhang et al. (2014)
	Impedance Spectroscopy	1.18×10^{-6}	1.18×10^{-6}-9.05×10^{-5}	18.8	Wu et al. (2010)
	Cyclic Voltammetry	10^{-7}	10^{-7}-10^{-3}	40	Kang et al. (2009)
Raman	SERs	9.12×10^{-8}	10^{-7}-10^{-4}	30	Ali et al. (2018)
Fluorescence	Pseudopaper ELISA	3.8×10^{-12}	1×10^{-11}-1×10^{-6}	50	Chi et al. (2017)
	Intensity	1.8×10^{-4}	1.8×10^{-4}-1.8×10^{-1}	30	This work
	FRET	5.1×10^{-4}	7.5×10^{-4}-6×10^{-2}	19	Li et al. (2017)
Chemiluminescent	Intensity	2×10^{-6}	5×10^{-7}-2.5×10^{-5}	17	Zhou et al. (2006)
Optofluidic laser	Intensity	1.8×10^{-10}	1.8×10^{-10}-1.8×10^{-5}	50	This work

[a] C_{max} and C_{min} are the maximum and minimum detectable concentration of IgG.

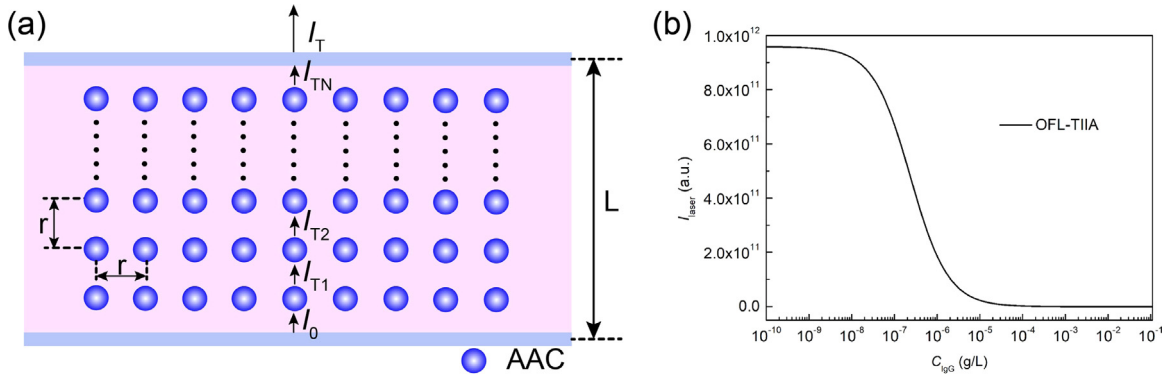

Fig. 5. (a) The ideal theoretical model for TIIA, in which the AAC and dye molecules are uniformly distributed in solution. L is the cavity length; r is the average distance between AAC molecules in the solution; I_0 is the incident light; and I_{T1}, I_{T2}, and I_{TN} are the transmitted light (i.e., scattering light at 0°) after one, two and N AAC molecules, respectively. I_T is the total transmitted light for a single cavity length. (b) Simulated laser intensity versus IgG concentration. In the simulations, $I_0 = 1$, $\varepsilon = 13.24\,nm^3$, $\lambda = 600\,nm$, $l = 1.1\,mm$, $a = 10^{-5}$, $R_1 = 0.995$, $R_2 = 0.915$, $\sigma = 6 \times 10^{-16}\,cm^2$, $\tau_{eff} = 2.6\,ns$, $g = 5 \times 10^5\,m^{-1}$, $n = 1.46$, and $Q = 10^6$ are used. This numerical simulation only qualitatively reflects the trend of the laser intensity changes with an increasing concentration of IgG.

frequency, σ is the fluorophore absorption cross-section, and τ_{eff} is the effective lifetime or recovery time for the transition). g, α_0, α_s and L are the unsaturated gain coefficient, internal cavity loss coefficient ($\alpha_0 = 2\pi n/\lambda Q$), scattering coefficient from the AACs, and the cavity length, respectively.

According to numerical simulations based on Eq. (3), the intensity of the laser decreases with the AAC-induced loss (Fig. 5b), which can qualitatively describe the trend of OFL-TIIA and is in agreement with the experimental observations (Fig. 4b). In accordance with laser/fluoresce theory, the output of the laser primarily originates from the multiple round-trip of the oscillation (multiple scattering), while that of fluorescence is mainly from a few oscillations of photons (few scattering). Therefore, the laser amplification effect contributes to the improved LOD of the standard curve on a semi-logarithmic scale, i.e., the sensitivity. Therefore, in addition to the CEF, the amplification effect of the laser further enhanced the sensitivity. Ultimately, an unprecedented LOD was achieved by OFL-TIIA.

4. Conclusion

An optofluidic laser turbidimetric inhibition immunoassay with a high sensitivity has been developed to analyze proteins. The antigen-antibody complexes from a commercial IgG TIIA kit were mixed with the optofluidic gain material in a Fabry-Perot laser cavity. The IgG concentration was detected by monitoring the optofluidic laser output. Because of the amplification effect of the laser, an extensive dynamic range of five orders of magnitude along with an LOD of 1.8×10^{-10} g/L was achieved. The unprecedented sensitivity of OFL-TIIA would enable the detection of biomarkers for the early diagnosis of diseases that were impossible for traditional TIIA. This improvement made up for the fatal weakness of traditional TIIA, which may refresh the extension of TIIA to widespread applications. In addition to the high sensitivity, this technology also minimizes the sample volume by almost 1000-fold and thus lowers the cost for each test. The homogeneous reaction, with a short molecule-molecule distance for diffusion, allows the molecules to attach to others in a short time and enables a rapid assay (< 20 min). With all these advantages, OFL-TIIA provides a powerful technological platform for disease diagnostics. Considering the abundance of commercial TIIA kits and the many TIIA kits under development, further expansion of TIIA applications is highly expected.

CRediT authorship contribution statement

Xi Yang: Methodology, Investigation, Validation, Formal analysis, Data curation, Writing - original draft. **Wenxiong Shu:** Investigation, Formal analysis, Writing - review & editing. **Yanqiong Wang:** Investigation, Writing - review & editing. **Yuan Gong:** Conceptualization, Methodology, Formal analysis, Writing - original draft, Resources, Funding acquisition. **Chaoyang Gong:** Validation, Formal analysis, Writing - review & editing. **Qiushu Chen:** Writing - review & editing. **Gang-Ding Peng:** Writing - review & editing. **Xudong Fan:** Supervision, Writing - review & editing. **Yun-Jiang Rao:** Writing - review & editing, Resources, Funding acquisition.

Acknowledgements

We acknowledge the financial support from the National Natural Science Foundation of China (61875034 and 61575039), the 111 Project (B14039), and the National Science Foundation (DBI-1451127).

Declaration of interests

The authors declare that they have no known competing financial interests or personal relationships that could have appeared to influence the work reported in this paper.

Appendix A. Supporting information

Supplementary data associated with this article can be found in the online version at doi:10.1016/j.bios.2019.02.013.

References

Ali, A., Hwang, E.Y., Choo, J., Lim, D.W., 2018. Sens. Actuators B 255, 183–192.
Arango, F.B., Christiansen, M.B., Gersborg-Hansen, M., Kristensen, A., 2007. Appl. Phys. Lett. 91, 223503–223505.
Chan, D.W., 1995. Anal. Chem. 67, 519R–524R.
Chen, Q., Chen, Y.C., Zhang, Z., Wu, B., Coleman, R., Fan, X., 2017a. Lab Chip 17, 2814–2820.
Chen, Y.C., Tan, X., Sun, Q., Chen, Q., Wang, W., Fan, X., 2017b. Nat. Biomed. Eng. 1, 724–735.
Chen, Y.C., Chen, Q., Wu, X., Tan, X., Wang, J., Fan, X., 2018. Lab Chip 18, 1057–1065.
Chi, J., Gao, B., Sun, M., Zhang, F., Su, E., Liu, H., Gu, Z., 2017. Anal. Chem. 89, 7727–7733.
Culver, H.R., Sharma, I., Wechsler, M.E., Anslyn, E.V., Peppas, N.A., 2017. Analyst 142, 3183–3193.
Deleo, D.E., Lee, I.R., Wetherall, J.D., Newman, D.J., Medcalf, E.A., Price, C.P., 1991. Clin. Chem. 37, 527–531.
Dhami, S., Mello, A.J.D.M., Rumbles, G., Bishop, S.M., Phillips, D., Beeby, A., 1995. Photochem. Photobiol. 61, 341–346.
Dong, S., Tong, M., Zhang, D., Huang, T., 2017. Sens. Actuators B 251, 650–657.
Fan, X., Yun, S.H., 2014. Nat. Methods 11, 141–147.
Ferreria, P., Price, C.P., 1974. Clin. Chim. Acta 55, 259–262.
Gather, M.C., Yun, S.H., 2011. Nat. Photonics 5, 406–410.
Gersborg-Hansen, M., Kristensen, A., 2006. Appl. Phys. Lett. 89, 103518–103520.
Gong, C., Gong, Y., Chen, Q., Rao, Y.J., Peng, G.D., Fan, X., 2017a. Lab Chip 17, 3431–3436.
Gong, C., Gong, Y., Oo, M.K.K., Wu, Y., Rao, Y., Tan, X., Fan, X., 2017b. Biosens. Bioelectron. 96, 351–357.
Gong, C., Gong, Y., Zhang, W.L., Wu, Y., Rao, Y.J., Peng, G.D., Fan, X., 2018. IEEE J. Sel. Top. Quantum Electron. 24, 0900206.
Hall, B.G., Acar, H., Nandipati, A., Barlow, M., 2013. Mol. Biol. Evol. 31, 232–238.
Harmoinen, A., Perko, M., Gronroos, P., 1981. Clin. Chim. Acta 111, 117–120.
Hillstrom, A., Hagman, R., Tvedten, H., Kjelgaard-Hansen, M., 2014. Vet. Clin. Pathol. 43/2, 235–243.
Holownia, P., Perez-Amodio, S., Price, C.P., 2001. Anal. Chem. 73, 3426–3431.
Humar, M., Yun, S.H., 2015. Nat. Photonics 9, 572–577.
Jiang, W., Xin, W., Xun, S., Chen, S., Gao, X., Liu, Z., Tian, J., 2017. Sens. Actuators B 249, 142–148.
Kang, H.J., Aziz, M.A., Jeon, B., Jo, K., Yang, H., 2009. Electroanalysis 21, 2647–2652.
Kjelgaard-Hansen, M., Jensen, A.L., Kristensen, A.T., 2004. Vet. Clin. Pathol. 33, 139–144.
Lacey, S., White, I.M., Sun, Y., Shopova, S.I., Cupps, J.M., Zhang, P., Fan, X., 2007. Opt. Express 15, 15523–15530.
Li, C., Zou, J., Li, Q., Chang, Y., Zhang, Y., Tu, L., Liu, X., Xue, B., Zhao, H., Zhang, H., Kong, X., 2017. Biosens. Bioelectron. 92, 335–341.
Li, R., Wu, K., Liu, C., Huang, Y., Wang, Y., Fang, H., Zhang, H., Li, C., 2014. Anal. Chem. 86, 5300–5307.
Li, Z., Zhang, Z., Emery, T., Scherer, A., Psaltis, D., 2006. Opt. Express 14, 696–701.
Li, Z., Zhou, W., Luo, M., Liu, Y., Tian, J., 2015. Opt. Express 23, 10413–10420.
Libby, R.L., 1938. J. Immunol. 34, 269–279.
Mashazi, P., Tetyana, P., Vilakazi, S., Nyokong, T., 2013. Biosens. Bioelectron. 49, 32–38.
Montes, R., Cespedes, F., Baeza, M., 2016. Biosens. Bioelectron. 78, 505–512.
Morin, I., Askin, S.P., Schaeffer, P.M., 2011. Analyst 136, 4815–4821.
Nishimura, A., Sawai, T., 2006. Clin. Chim. Acta 371, 163–168.
Otsuji, S., Shibata, H., Umeda, M., 1982. Clin. Chem. 28/10, 2121–2124.
Rosales-Rivera, L.C., Acero-Sanchez, J.L., Lozano-Sanchez, P., Katakis, I., O'Sullivan, C.K., 2012. Biosens. Bioelectron. 33, 134–138.
Shopova, S.I., Zhou, H., Fan, X., 2007. Appl. Phys. Lett. 90, 221101–221103.
Siegman, A.E., 1986. Lasers. University Science Books, California, pp. 477.
Srihirun, S., Sriwantana, T., Unchern, S., Kittikool, D., Noulsri, E., Pattanapanyasat, K., Fucharoen, S., Piknova, B., Schechter, A.N., Sibmooh, N., 2012. PLoS One 7, e30380.
Subramanian, P., Motorina, A., Yeap, W.S., Haenen, K., Coffinier, Y., Zaitsev, V., Niedziolka-Jonsson, J., Boukherroub, R., Szunerits, S., 2014. Analyst 139, 1726–1731.
Thanh, N.T.K., Rosenzweig, Z., 2002. Anal. Chem. 74, 1624–1628.
Whicher, J.T., Price, C.P., Spencer, K., 1982. Crit. Rev. Clin. Lab. Sci. 18, 213–260.
Wilson, M.S., 2005. Anal. Chem. 77, 1496–1502.
Wu, X., Khaing, Oo, M.K., Reddy, K., Chen, Q., Sun, Y., Fan, X., 2014. Nat. Commun. 5, 3779–3785.
Wu, Z., Cao, Z., Zeng, J.L., Zhang, L., Chu, X., Shen, G.L., Yu, R.Q., 2010. Anal. Sci. 26, 1001–1006.
Wu, Z., Shen, G., Xie, L., Yu, R., 2000. Sens. Actuators B 71, 99–105.
Zhang, D., Sun, Y., Wu, Q., Ma, P., Zhang, H., Wang, Y., Song, D., 2016. Talanta 146, 364–368.
Zhang, S., Li, R., Liu, X., Yang, L., Lu, Q., Liu, M., Li, H., Zhang, Y., Yao, S., 2017. Biosens. Bioelectron. 92, 457–464.
Zhang, X., Shen, G., Sun, S., Shen, Y., Zhang, C., Xiao, A., 2014. Sens. Actuators B 200, 304–309.
Zhou, Y., Zhang, Y., Lau, C., Lu, J., 2006. Anal. Chem. 78, 5920–5924.
Zhu, J.M., Shi, Y., Zhu, Q., Yang, Y., Jiang, F.H., Sun, J., Zhao, W.H., Han, X.T., 2017. Lab Chip 17, 4025–4030.